applied sciences

MDPI

Article

Performance Evolution of Recycled Aggregate Concrete under the Coupled Effect of Freeze–Thaw Cycles and Sulfate Attack

Pu Jia [1], Lang Li [2], Jin Zhou [1], Di Zhang [1], Zhongwei Guan [3,4], Jiangfeng Dong [2,*] and Qingyuan Wang [2,3,*]

[1] School of Mechanical Engineering, Xi'an Jiaotong University, Xi'an 710049, China; p.jia6@xjtu.edu.cn (P.J.); jin.zhou@xjtu.edu.cn (J.Z.); zhangdi0719@xjtu.edu.cn (D.Z.)
[2] Failure Mechanics & Engineering Disaster Prevention and Mitigation Key Laboratory of Sichuan Province, College of Architecture & Environment, Sichuan University, Chengdu 610065, China; li_lang@outlook.com
[3] School of Architecture and Civil Engineering, Chengdu University, Chengdu 610106, China; zguan@liv.ac.uk
[4] School of Engineering, University of Liverpool, Liverpool L69 3GQ, UK
* Correspondence: dongjf@scu.edu.cn (J.D.); wangqy@scu.edu.cn (Q.W.)

Abstract: The high porosity of recycled coarse aggregate, which results in recycled aggregate concrete (RAC) more vulnerable to freeze–thaw (FT) damage and chemical attack, is a dominant factor that limits the industrialization of recycled aggregate concrete in civil engineering. This paper presents an experimental study on the combined effects of FT damage and sulfate attack on mechanical properties of high-performance RAC. The influence of the combined damage on the mass, solution-filled pore volume, dynamic elastic modulus, compressive strength, splitting tensile strength and fracture energy of RAC was studied. Results showed that the water-exposed FT cycles would result in more severe deterioration in the mass loss, elastic modulus and compressive strength, while for the sulfate-exposed FT cycles, the splitting tensile strength and fracture energy have more significant degradation. Moreover, compared with compressive strength, deterioration in splitting tensile strength is more severe. The maximum losses in compressive and splitting tensile strength were 28.7% and 35%, respectively. The fracture energy showed an increasing trend to 60 FT cycles, followed by an overall decrease to 180 FT cycles. The fracture energy exhibits a maximum increment of about 45% and 39% for water- and sulfate-exposed samples, respectively, after being subjected to 60 FT cycles. The analysis of failure modes of coarse aggregate has revealed that FT damage results in a significant deterioration in the binding force of mortar. After being subjected to 180 FT cycles, the area percentage of pulled-out failure was increased from 7.3% to larger than 17.3%.

Keywords: recycled aggregate concrete; freeze–thaw durability; sulfate attack; strength; fracture energy

Citation: Jia, P.; Li, L.; Zhou, J.; Zhang, D.; Guan, Z.; Dong, J.; Wang, Q. Performance Evolution of Recycled Aggregate Concrete under the Coupled Effect of Freeze–Thaw Cycles and Sulfate Attack. *Appl. Sci.* **2022**, *12*, 6950. https://doi.org/10.3390/app12146950

Academic Editor: Lorena Zichella

Received: 15 June 2022
Accepted: 5 July 2022
Published: 8 July 2022

1. Introduction

As the most widely used construction material, concrete represents a large source of natural resources depletion and global greenhouse gas emissions [1,2]. For efficient waste management, recycled coarse aggregate (RCA) is a promising sustainable construction material [3]. Although there is fast progress in research related to construction and demolition wastes recycling, it is not very satisfactory in many countries [4,5] due to the inferior properties of recycled aggregate concrete in comparison to conventional concrete. In recent years, many studies have been carried out to improve the mechanical properties of RAC, using chemical admixtures, active mineral additives and fibres [6–8]. Bui et al. [9] studied the properties of RAC based on a new combination method, in which only large-size recycled aggregate particles were replaced by ordinary aggregate in coarse aggregates. The study confirmed that the large coarse aggregate plays a crucial role in RAC performance. Using the new combination method, the percentage of recycled coarse aggregate in the concrete could be up to 50%, with the compressive strength being changed slightly compared to

that of the ordinary concrete. Bravo et al. [10] investigated the efficiency of the superplasticizer on the mechanical properties of RAC and confirmed the efficiency of polycarboxylic superplasticizer to enhance the mechanical properties of RAC to a satisfactory level.

By improving the properties of mortar and interfacial transition zones (ITZs), the mechanical properties of RAC could be significantly improved. Nevertheless, inferior properties of RCA, such as high porosity, high water absorption, low density and low strength, still exist. Pepe et al. [11] found that the mechanical performance of RAC could be predicted by considering only water absorption capacity to quantify the "quality" of recycled coarse aggregate. Dilbas et al. [12] studied the permeability of RAC, and they further indicated the significant reduction of RAC permeability by adding 10% silica fume to the concrete mixture. On the other hand, fluid ingress is a primary factor that influences the freeze–thaw damage in concrete and is still one of the most important durability problems for concrete [13]. When the degree of saturation of water exceeds 86–88%, the freeze–thaw damage is inevitable, with or without air entrainment, even by exposure to a few freeze–thaw cycles [14].

The high porosity of recycled coarse aggregate results in high water absorption and less resistance to chemical attacks in comparison to ordinary concrete. Kou and Poon [15] studied the effect of parent concrete quality on the properties of RAC and recorded an increase of chloride-ion penetration in the presence of recycled coarse aggregate compared to ordinary concrete. This phenomenon was also confirmed through the evaluation of the sulfate resistance of concrete with recycled coarse aggregate and natural aggregate [16]. Indeed, much research has been conducted on the durability of RAC under the freeze–thaw cycle or sulfate attack [17–19]. Comparatively, limited studies were carried out on the combined effects of chemical attacks (chloride corrosion, sulfate attack) and freeze–thaw damage [20–23]. For instance, Farnam et al. [24] studied the damage development in concrete exposed to deicing salt and reported that ice formation was the main reason causing damage for mortar exposed to low concentration $MgCl_2$ solutions (<10% by weight), while the deterioration was most likely due to chemical attacks at higher concentrations ($\geq$10% by weight).

The area of saline-alkali land in China ranks third in the world. These saline-alkali lands are mainly located in the northwestern parts of China, such as Xinjiang, Ningxia and Inner Mongolia, and northeast China [25]. Most of these regions are also characterized by a high altitude/latitude and low winter temperature. Consequently, the combined damage is more relevant to in-service conditions than the classical FT cycles and sulfate immersion tests. The sulfate attack of the solution to the concrete is affected by a lot of factors. Thaumasite is more likely to form at low temperatures of around 5 °C, accompanied by a reduction in the binding ability of cement. There has been extensive experimental research on the mechanical properties [26–29] and durability of RAC under freeze–thaw cycles or sulfate attacks. Additionally, some attempts have been made to study the combined effects of chemical attacks and FT damage on ordinary concrete. However, regarding the influence of sulfate attack and FT damage on the tensile and fracture properties of RAC, there is limited published research work in this respect. To close this knowledge gap, the present study aimed to investigate the influence of the combined FT damage and sulfate attack on the mechanical properties of high-performance RAC. The work focused on the influence of the combined damage on mass, solution-filled pore volume, dynamic elastic modulus (E_{dym}), compressive strength, splitting tensile strength and fracture energy of RAC. In addition, the mid-span fracture surface of prisms was analyzed to obtain insight into the failure mode of aggregate in relation to FT damage. Moreover, XRD analyses for RAC exposed to combined FT damage and sulfate attack were carried out. The present study provides valuable outcomes and investigations for the potential use of high-performance RAC in cold regions.

2. Materials and Methods

2.1. Materials and Specimens

The mixture properties of RAC are shown in Table 1. RCA was produced using crushed and sieved waste pavement concrete collected from pavement renovation. The sizes of recycled coarse aggregate and natural coarse aggregate (NCA) were all between 4.75 mm and 19 mm, while the water absorption ratio of RCA was 8.5%. Fly ash (FA), which takes 20% of the gelatinizing agent by weight, was used as a replacement of cement and an active mineral additive here. The gradation curves of fly ash, fine aggregate, NCA and RCA are shown in Figure 1. In addition, a polycarboxylic superplasticizer (SP) was also used to improve the workability of RAC. The properties of the polycarboxylic superplasticizer are shown in Table 2. Both FA and SP were used to improve the mechanical properties of RAC. Before casting, the RCA was immersed in water for 3 days to be saturated. After casting, all specimens were cured in water at 20 °C for 3 months and, therefore, the strength developed during the subsequent testing period can be ignored.

Table 1. Mix properties of concrete (kg·m^{-3}).

Cement	Sand	NCA	RCA	FA	SP	Water	w/c	w/b
440	610	620	620	110	1.1	165	0.5	0.4

Note: The w/c and w/b are the total water-to-cement and water-to-binder ratios. NCA is natural coarse aggregate.

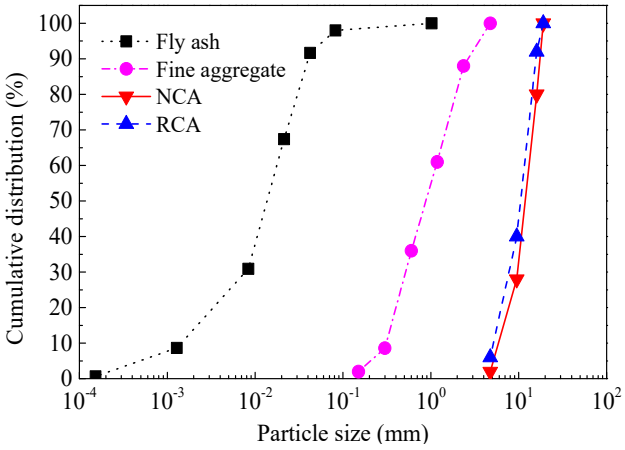

Figure 1. The gradation curves for fly ash, fine aggregate, NCA and RCA.

Table 2. Properties of the polycarboxylic superplasticizer.

Appearance	Water-Reducing Ratio	Moisture Content	Bulk Density/kg.m^{-3}
Grey powder	≥25%	≤5.0%	500~700
PH Value (20 °C, 10% Aqueous Solutions)	**Chloride Ions Content**	**Sodium Sulfate Content**	**Alkali Content**
6~8	≤0.03%	≤3.0%	≤0.5%

According to the Standard Test Method of GB/T 50082-2009 [30], beam specimens with dimensions of 100 mm × 100 mm × 400 mm were adopted in the FT tests. Consequently, a notched beam with the same dimensions was adopted to investigate the fracture behaviour of RAC after being exposed to 60, 90, 120, 150 and 180 FT cycles. In the three-point bending test, the span-to-depth ratio and notch-to-depth ratio were 3 and 0.3, respectively (Figure 2).

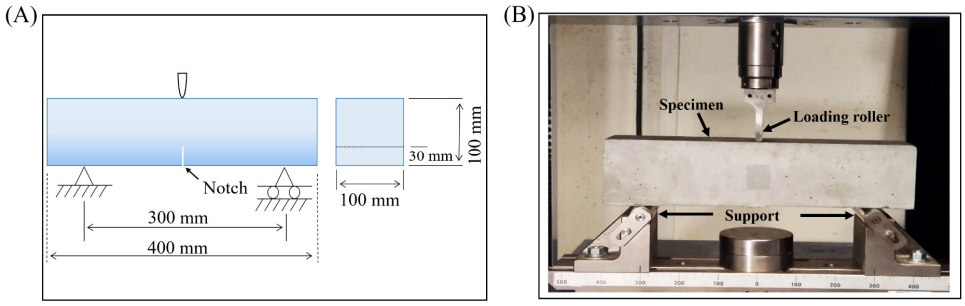

Figure 2. Schematic of the notched beam (**A**) and experimental apparatus of the notched beam (**B**) under quasi-static three-point bending test.

2.2. Freeze–Thaw Tests

The rapid freeze–thaw tests were conducted on the specimens saturated with water or sulfate solution using a fast freeze–thaw test machine. According to GB/T 50082-2009 [30], the internal temperature of specimens was controlled to vary between 5 ± 2 °C and −15 ± 2 °C in nearly 4 h for each cycle. The cycle started at 5 °C and cooled down to −15 °C in 2 h, followed by a 10 min isothermal stage at −15 °C. Then it was heated up to 5 °C in 1.5 h and maintained for 10 min again. The internal temperature of freezing–thawing specimens is shown in Figure 3.

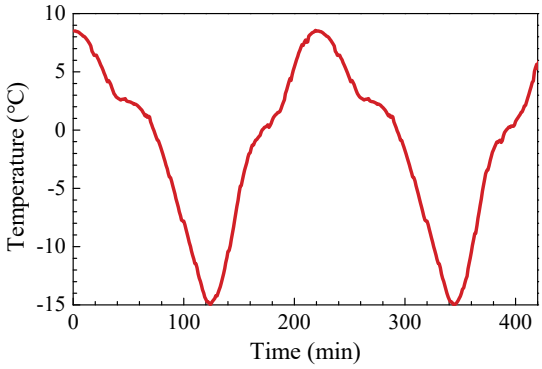

Figure 3. Internal temperature of notched beam in freeze–thaw cycles.

2.3. Mass Change, Water Absorption and Internal Damage

Before freeze–thaw testing, the specimens were dried in a drying oven at 60 °C for 24 h. This relatively low temperature was selected to avoid potentially destroying the pore structure at a high temperature [31] and to decrease the influence of the drying process on the water absorption of the specimens. It was followed by measuring an oven-dried mass and E_{dym}. The specimens were immersed in sulfate solution (or water) for a week [32] as a presaturation stage; then the saturated surface dry mass was recorded. These natural saturated specimens were then subjected to 60, 90, 120, 150 and 180 FT cycles, during which they were exposed to water or sulfate solution. Sodium sulfate solution at 5% (by mass) was used in the present study as sulfate solution. After FT testing, the saturated mass, oven-dried mass and E_{dym} were analyzed again to determine the frost damage.

The freeze–thaw induced mass loss (percent) of concrete specimens can be calculated by

$$\Delta m_N = (m_1 - m_2)/m_1 \times 100\% \quad (1)$$

where m_1 (g) and m_2 (g) are the mass before and after N freeze–thaw cycles, respectively.

As mentioned before, micro-cracks were developed with FT cycles and they provided additional paths for solution penetrating into the internal pores. Consequently, saturated water absorption provides an indirect way to quantify the development of micro-cracks [33,34],

which was also used in the present work to evaluate FT damage. The volume of solution-filled pores and voids (V, mm^{-3}) was calculated from the saturated mass (m_s, g) and oven-dried mass (m_d, g) using Equation (2):

$$V = (m_s - m_d)/\rho \quad (2)$$

where $\rho(g \cdot mm^{-3})$ is the density of water.

The extent of internal damage caused by freeze–thaw cycles can be regularly evaluated by a relative dynamic elastic modulus (RDEM). Here, a damage parameter (1-RDEM) was used to assess the frost damage, which can be expressed by Equation (3):

$$D = 1 - E_{dyn,FT}/E_{dyn,0} \quad (3)$$

where $E_{dyn,0}$ (GPa) and $E_{dyn,FT}$ (GPa) are the dynamic elastic modulus before and after FT cycles.

2.4. Mechanical Property Tests

Three-point bending tests (TPBT), referring to the RILEM Technical Committee 50-FMC [35], were conducted using a 100 kN electronic universal testing machine (SHIMADZU). The beam specimen had a dimension of 100 mm × 100 mm × 400 mm. The notched specimens were loaded until failure at a crosshead displacement rate of 0.1 mm · min^{-1}. A 2000 kN electro-hydraulic testing machine was used for compression and splitting tests. According to GB/T 50081-2002 [36], the stress rate was set to 0.5 and 0.05 MPa · s^{-1} in compression and splitting tests, respectively. The cubic specimens were cut to a size of 100 mm × 100 mm × 100 mm from the fractured prism specimens, which was to ensure that the corresponding compression and splitting tensile results were obtained from concrete samples with the same properties [37]. It should be noted that the shear forces near the supports in the bending test were all less than 4 kN, which means that there was hardly any influence on the measured strength of the cubic specimens.

The fracture energy of concrete, G_F, is a fundamental fracture parameter used to indicate its crack resistance in fracture and in crack analysis. It can be defined as the amount of energy required to produce a unit area of a crack. Following the RILEM [35] recommendations, fracture energy can be determined from the experimental load-deflection curve using Equation (4):

$$G_F = (W_0 + mg\delta_0)/A \quad (4)$$

where W_0 is the total area under the load-deflection curve, m is the mass of the beam between the supports, δ_0 is the mid-span deflection of the beam upon failure, $g = 9.81$ m · s^{-2} is the gravitational acceleration and A is the area of the ligament. Here, $A = t \cdot h$, where t is the width of the beam and h (equal to 70 mm) is the depth of the ligament.

3. Results and Discussion

The effects of FT damage on physical properties including mass loss, water absorption and dynamic elastic modulus were studied. Then, the results obtained in the TPBT, compression tests and splitting tests are discussed, respectively, followed by the XRD analyses.

3.1. Mass Loss and Water Absorption

According to the results of previous studies [14,22], the normalized amount of water absorbed is proportional to the square root of time, and after immersing in water for 7 days, the slope is between 0.026 and 0.033 [14]. Thus, the change of water absorption in this study may be seen as a consequence of FT damage.

The recorded masses and calculated solution-filled pore volumes at different FT cycles and exposure conditions are listed in Table 3. The calculated saturated and oven-dried mass losses at different FT cycles are shown in Figure 4. It is clear that saturated and oven-dried specimens exposed to water have more mass loss than those exposed to sulfate

solution. This result indicates that FT cycles under water exposure may cause more serious damage to the concrete. However, the oven-dried mass loss (Figure 4B) for both groups of specimens increased with the increase of FT cycles, which is in accordance with the damage accumulation caused by FT cycles increasing. However, the saturated mass loss (Figure 4A) was not stabilized during the FT tests. This indicates that oven-dried tests are more suitable for assessing FT damage than the saturated mass one.

Table 3. Mass and solution-filled pore volume of notched beams subjected to freeze–thaw cycles.

Specimen	FT Cycles	m_{1s} (g)	m_{1d} (g)	m_{2s} (g)	m_{2d} (g)	V_1 (mm^3)	V_2 (mm^3)
0 (W0/S0)	0	-	-	-	-	-	-
W60	60	9306	9217	9270	9178	89	92
W90	90	9087	8999	9023	8931	88	92
W120	120	9539	9474	9474	9399	65	75
W150	150	9101	9018	9041	8924	83	117
W180	180	9047	8955	8976	8813	92	163
S60	60	9143	9048	9116	9029	95	87
S90	90	9298	9224	9273	9205	74	68
S120	120	9106	9019	9083	8985	87	98
S150	150	9060	8996	9031	8944	64	87
S180	180	9206	9127	9146	9033	79	113

Note: "W" and "S" correspond to exposure of the specimens to water or sulfate solution, respectively, while numbers represent the FT cycles. m_s, m_d and V are saturated mass, oven-dried mass and solution-filled pore volume, respectively; the subscripts 1 and 2 indicate before and after FT cycles, respectively.

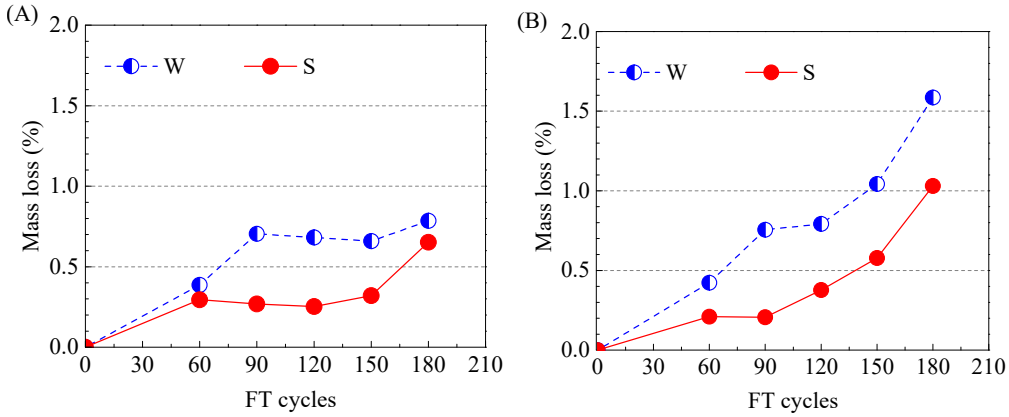

Figure 4. Saturated mass loss (**A**) and oven-dried mass loss (**B**) at different FT cycles of water saturated (W) and sulfate attack (S) RAC.

In addition, FT causes the development of micro-cracks, which eventually results in the change of solution absorption [33]. The relative solution-filled pore volume, i.e., the ratio of solution-filled pore volume after being subjected to FT cycles to the one before FT cycles, is shown in Figure 5. For water-exposed specimens (W), the relative solution-filled pore volume was always larger than one, which confirms that FT results in an increase in solution-filled pore volume. A similar phenomenon was also recorded in sulfate-exposed specimens (S) after being subjected to 120 FT cycles or more. However, for sulfate-exposed specimens, there was hardly any decrease in their pore volumes from 60 to 90 FT cycles. This may be attributed to the precipitation of the synthesized ettringite and thaumasite, a common phenomenon of sulfate attack, which results in the decrease of pore volume [38–40].

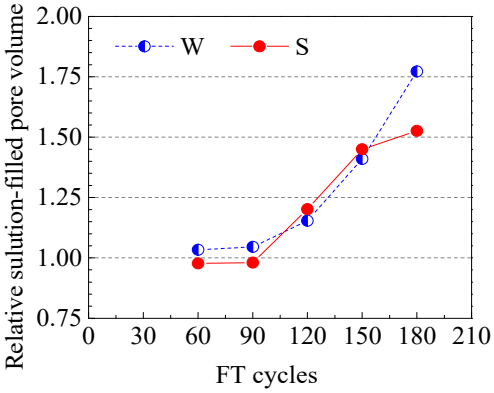

Figure 5. Changes of solution-filled pore volume of water-exposed (W) and sulfate-exposed (S) RAC samples at different freeze–thaw cycles.

Different from the mass loss, the differences in solution-filled pore volume between water- and sulfate-exposed specimens was small at lower FT cycles, while 180 cycles resulted in a 16.1% increase of pore volume in the water-exposed sample (Figure 5). For specimens subjected to 120 and 150 FT cycles, the pore volume changes of the sulfate solution exposure group were marginally higher (4.1% and 2.9%, respectively) than that of their water exposure counterparts. A small amount of spalling caused by salt crystallization during oven-drying results in a smaller dried mass and may also have led to this trend.

3.2. Dynamic Elastic Modulus

The calculated damage parameters at different FT cycles and exposure conditions are listed in Table 4. The effects of different FT cycles on the damage parameter of water- and sulfate-exposed samples are shown in Figure 6. For RAC, specimens subjected to water-exposed FT cycles showed a much more severe elastic modulus deterioration at all studied FT cycles when compared to the sulfate-exposed ones. For water- and sulfate-exposed specimens, the loss in elastic modulus (damage parameters) reached their maximum values (24.6% and 21.5%, respectively) after being subjected to 180 FT cycles. For water-exposed specimens subjected to 120 or fewer FT cycles, the damage parameter increasingly grew with FT cycles. However, when subjected to 120 or more cycles, the growth of the damage parameter was in a decreasing manner. Compared to the water-exposed specimens, the increase of the damage parameter of sulfate-exposed ones displayed a contrary tendency.

Table 4. Mechanical properties of notched beams subjected to freeze–thaw cycles.

Specimen	FT Cycles	D	f_c (MPa)	f_t (MPa)	G_F (J·mm^{-2})
0 (W0/S0)	0	0	59.5	4.0	300.9
W60	60	0.068	56.2	3.5	437.1
W90	90	0.109	51.1	3.2	326.7
W120	120	0.173	47.5	3.0	342.5
W150	150	0.211	44.3	2.9	309.2
W180	180	0.246	42.4	2.6	274.1
S60	60	0.048	57.8	3.6	417.9
S90	90	0.073	53.5	3.3	386.1
S120	120	0.092	51.2	3.1	322.2
S150	150	0.15	49.8	3.0	252.1
S180	180	0.215	46.1	2.6	254.1

Note: D is damage parameter; f_c, f_t *and* G_F are compressive strength, splitting tensile strength and fracture energy, respectively.

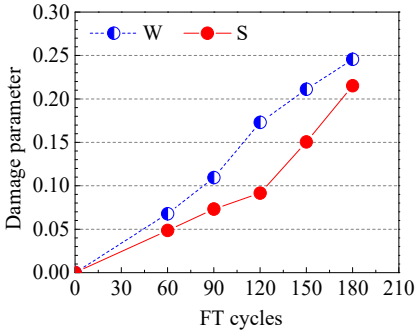

Figure 6. Evolutions of damage parameter of water-exposed (W) and sulfate-exposed (S) RAC samples at different freeze–thaw cycles.

The more severe deterioration in the elastic modulus was also seen in the specimen exposed to deicing salt solution, which showed a difference in liquid pressure caused by the water and salt solution [21,24]. Moreover, the study conducted by Zeng et al. [21] showed that the sodium chloride in solution tends to decrease the ice formation, and, as a result, the maximum liquid pressure decreases. Here, sodium sulfate may have similar effects on pore pressure with respect to the deicing salt.

3.3. Compressive Strength and Splitting Tensile Strength

In order to understand the strength degradation under different FT cycles, tests on both compressive strength and splitting tensile strength were undertaken. The measured strengths at different FT cycles and exposure conditions are listed in Table 4. Figure 7A shows the dimensionless value of strength, i.e., relative residual compressive and splitting tensile strength, against FT cycles.

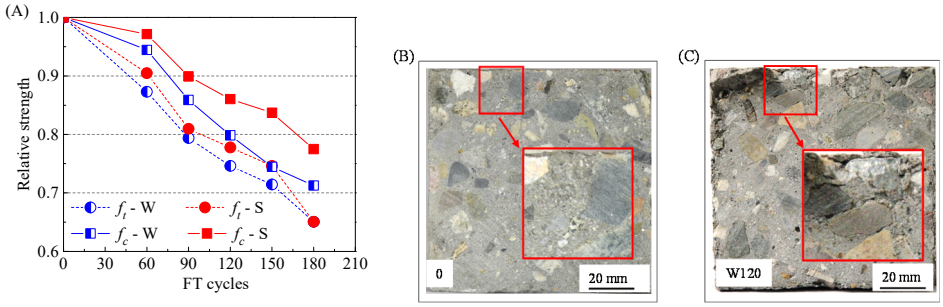

Figure 7. Evolutions of residual strength (**A**) and interfacial transition zones (**B**,**C**) at different freeze–thaw cycles.

In RAC subjected to sulfate–FT damage, the loss in compressive strength was smaller compared to the ones subjected to water–FT damage. For water- and sulfate-exposed samples subjected to 180 FT cycles, the residual compressive strengths were about 71% and 78% of the original strength, respectively. The residual strength of W180 was about 92% of that of S180. This phenomenon was also confirmed by Jiang [41] through studying the durability of high-performance concrete, which was subjected to the same exposed conditions.

Moreover, for both RAC in this study and high-performance concrete (w/c = 0.56) in [41] subjected to FT cycles, their compressive strengths were in a pronounced linear relationship with FT cycles. Moreover, as a consequence of high porosity, the RCA concrete showed more loss in compressive strength compared with ordinary concrete in [41], despite adopting a lower w/b ratio.

However, for the splitting tensile strength of RAC tested in this study, slight differences were noticed between different exposed conditions. For both water- and sulfate-exposed samples subjected to 180 FT cycles, the residual splitting tensile strength was about 65%

of the original strength. For RAC subjected to sulfate–FT damage, except for 180 FT cycles, the loss in splitting tensile strength was smaller compared to the ones subjected to water–FT damage.

After subjected to 180 FT cycles, there was about a 35% decrease in splitting tensile strength, which is higher than the loss in compressive strength. Therefore, compared with the compressive strength, the tensile strength is more sensitive to FT damage. It is generally recognized that the interfacial bonding between aggregate and mortar is vital for the tensile strength. Figure 7B,C shows the cutting face of the control specimen (0) and the water-exposed specimen with 120 FT cycles (W120). For the FT-damaged specimen, macrocracks, which mainly developed in regions close to the surface, were observed in the interface between the aggregate and mortar. Therefore, damage in the interfacial transition zones (ITZs) also occurs during cyclic FT damage, which contributes to more-serious degradation in splitting tensile strength. The quantitative analysis of the deterioration in ITZs will be discussed in the following section.

3.4. Fracture Energy

Figure 8A shows the normalized fracture energy versus FT cycles, which were obtained by dividing the G_F with the control. Different from the loss in E_{dyn} and strength under FT damage, there was even an increase in the fracture energy for both water- and sulfate-exposed samples. The fracture energy showed an increasing trend to 60 FT cycles, followed by an overall decrease until 180 FT cycles. After being subjected to 60 FT cycles, the fracture energy showed a maximum increment of about 45% and 39% for water- and sulfate-exposed samples, respectively. Generally, for the sulfate-exposed specimens, the fracture energy decreases more sharply compared to that of water-exposed specimens. After being subjected to 180 FT cycles, there was about a 16% decrease in fracture energy for the sulfate-exposed specimen, which is higher than that of the water-exposed one (9%). Kazberuk et al. [42] reported a similar variation trend in the study of the effects of internal frost damage on the fracture energy of aerated and non-aerated concrete.

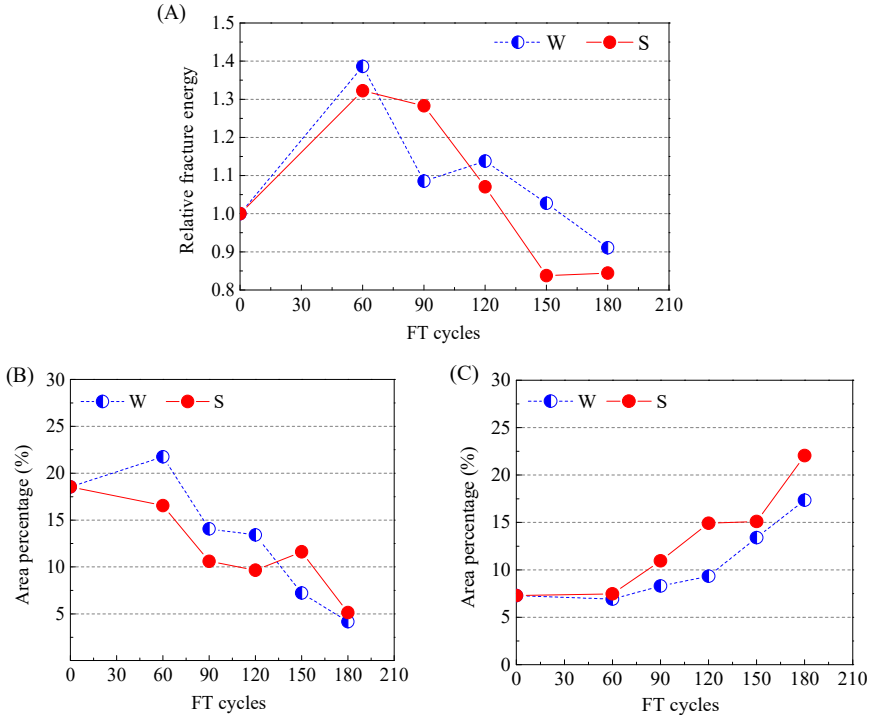

Figure 8. Evolution of fracture energy (**A**) and area percentage of aggregate splitting failure (**B**) and pulled-out failure (**C**) at different FT cycles.

The fracture energy, G_F, required for the creation of a fracture surface can be expressed as

$$G_F = 2(A_m \cdot \gamma_m + A_a \cdot \gamma_a + A_i \cdot \gamma_i) \quad (5)$$

where A is the area of fracture surface and γ represents the energy dissipated for the crack propagation, with the subscripts *m*, *a* and *i* indicating the matrix, aggregate and interface phases, respectively. Consequently, the fracture surface were analyzed to investigate the increase in G_F. The area percentage of different failure modes of aggregates were obtained using a MATLAB code. It is worth pointing out here that the fracture of mortar parts in RCA, mainly the crushed mortar, is considered as the mortar failure.

Figure 8B,C show the area percentage of different failure modes of aggregates with different FT cycles. In general, a noticeable increase in the interface damage (Figure 8C), which corresponds to a sharp decrease in the splitting damage (Figure 8B). For the control specimen with zero FT cycle, the area percentages of the fractured aggregate (Figure 8B) and interface failure (Figure 8C) were 18.5% and 7.3%, respectively. However, specimens subjected to 120 FT cycles in sulfate solution showed 9.6% and 14.9%, respectively. After being subjected to 180 FT cycles, the area percentage of splitting and pulled-out failure were around 5% and larger than 17.3% respectively. For pulled-out aggregate failure, specimens subjected to FT under sulfate-exposed showed a higher area percentage at all studied FT cycles when compared to the water-exposed ones. After being subjected to 180 FT cycles, the area percentage of pulled-out aggregate failure was 22.1% and 17.3% for the sulfate- and water-exposed specimens, respectively. This indicates that a significant deterioration in the binding force of mortar occurs during the cyclic FT damage. Compared to the area of ligament, the failure of the curved interface eventually results in a larger area of the fracture surface. However, the fracture energy is calculated based on the effective cross-section area (i.e., $t \cdot h$) and thus contributes to higher fracture energy.

3.5. The Relationship between Strength and Damage Parameter

Due to the compressive actions on the structural concrete, understanding the degradation of the compressive strength under FT cycles is essential for the effective utilization of concrete in cold regions. Moreover, tensile strength is a basic parameter in fracture calculation and simulation of concrete structures. Consequently, determination of strength under FT cycles is vital, which will contribute to the development of concrete performance models and service life tools, supporting a holistic approach for deterioration assessment [43]. For different FT cycles, the strength loss and damage parameters are shown in Figure 9. Damage parameter, compressive strength and split-tensile strength all showed a strong linear relationship with FT cycles. Therefore, for a given concrete subjected to FT cycles, the damage parameter can be used to predict the residual strength.

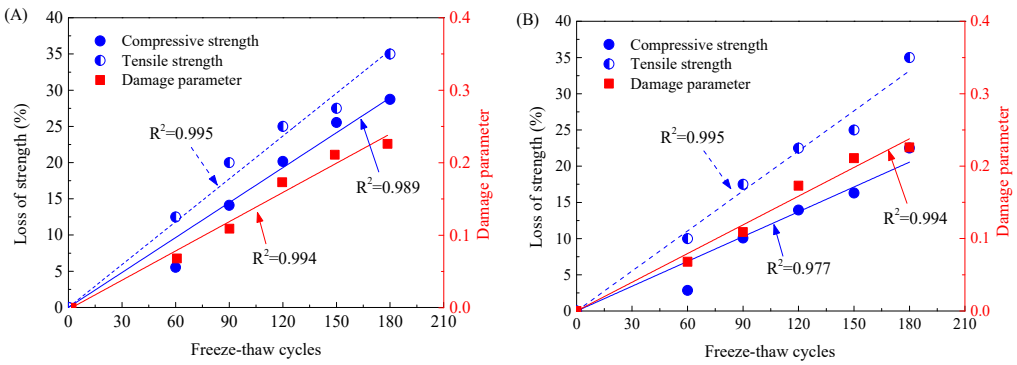

Figure 9. The relationship between strength loss and damage parameter for water-exposed (**A**) and sulfate-exposed (**B**) RAC.

For the specimen subjected to FT cycles, its residual strength can be expressed as;

$$\sigma_R = \sigma_0(1 - \alpha(1 - e^{\beta n})) \quad (6)$$

where σ_R and σ_0 are the residual and the original strength, respectively, while n is the number of FT cycles in strength prediction. The coefficients α and β can be calculated using Equations (7) and (8);

$$\alpha = (1 - \sigma_R(N)/\sigma_0)/(1 - E_{dyn,FT-N}/E_{dyn,0}) \quad (7)$$

And

$$\beta = \ln(E_{dyn,FT-N}/E_{dyn,0})/N \quad (8)$$

where N is the number of FT cycles in the experiment, $E_{dyn,0}$ and $E_{dyn,FT-N}$ are the dynamic elastic modulus before and after FT tests with N cycles. Here, the factor α, which approximately equals to one, reflects the relationship between the deterioration of strength and dynamic elastic modulus, while β indicates the effects of FT cycles on the dynamic elastic modulus. As dynamic elastic modulus has been widely studied for concrete with different mixture properties, it is convenient to determine those coefficients. For the RAC tested in the present study, $\alpha = 1.16$ and $\beta = 0.002$ can be utilized to predict the residual compressive strength of specimens subjected to water-saturated FT condition.

3.6. Analytical Techniques

The identification of potential products formed as a result of the chemical attack was further analyzed by XRD. Freeze–thaw damage of water-saturated concrete is a progress of physical attack. Hence, only sulfate-exposed specimen was analyzed by XRD.

The XRD patterns of specimens 0 and S150 are presented in Figure 10. Calcium carbonate could be observed in the XRD pattern of S150. It is in accordance with the fact that decomposition of thaumasite occurs at about 60 °C during oven drying treatment. In addition, the peak of ettringite was more obvious in specimen S150, which indicates that ettringite was also a corrosion product. Based on XRD analysis, it can be indicated that chemical sulfate attack proceeds within the FT tests exposed to sulfate solution exposure. Both thaumasite and ettringite are produced in sulfate attacked specimens. Although the lower temperature may significantly slow down the reaction rate between sulfate ions and hydration products, this chemical attack still needs to be considered in the long-term services of RAC.

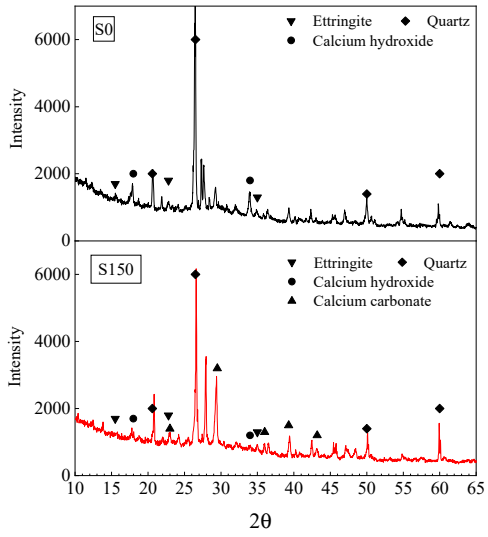

Figure 10. XRD patterns of RAC in control condition (S0) and subjected to sulfate-exposed FT cycles (S150).

4. Conclusions

The study has been undertaken to investigate the effects of FT damage on the mechanical properties of high-performance RAC. Both water- and sulfate-exposed conditions were considered. Based on the results presented, the following conclusions can be drawn:

(1) The oven-dried mass decreases linearly with FT cycles. However, the saturated mass fluctuates slightly during the tests. The loss of the oven-dried mass is more suitable for assessing FT damage than the saturated mass.

(2) The water-exposed FT cycles would result in more severe deterioration in mass loss, elastic modulus and compressive strength, while for the sulfate-exposed FT cycles, the splitting tensile strength and fracture energy have more serious degradation. Compared with compressive strength, deterioration in splitting tensile strength is more severe. The maximum losses in compressive and splitting tensile strength are 28.7% and 35%, respectively.

(3) The fracture energy showed an increasing trend to 60 FT cycles, followed by an overall decrease to 180 FT cycles. It indicated a maximum increment of about 45% and 39% for water- and sulfate-exposed samples, respectively, after being subjected to 60 FT cycles. The analysis of failure modes of coarse aggregate reveals that FT damage results in a significant deterioration in the binding force of mortar. After being subjected to 180 FT cycles, the area percentage of pulled-out failure was increased from 7.3% to larger than 17.3%.

Author Contributions: Conceptualization, P.J.; methodology, P.J. and L.L.; validation, P.J. and J.D.; investigation, P.J. and D.Z.; resources, J.D.; writing—original draft preparation, P.J.; writing—review and editing, J.Z. and Z.G.; visualization, P.J.; supervision, Z.G. and Q.W.; project administration, J.D. and Q.W.; funding acquisition, P.J. and Q.W. All authors have read and agreed to the published version of the manuscript.

Funding: The authors are sincerely grateful for the financial support provided by the Natural Science Basic Research Program of Shaanxi (Program No. 2021JQ-004) and the 2021 Open Project of Failure Mechanics and Engineering Disaster Prevention, Key Lab of Sichuan Province, No. FMEDP202114.

Institutional Review Board Statement: Not applicable.

Informed Consent Statement: Not applicable.

Data Availability Statement: Data are available by request from the corresponding author.

Conflicts of Interest: The authors declare no conflict of interest.

References

1. Meyer, C. The greening of the concrete industry. *Cem. Concr. Compos.* **2009**, *31*, 601–605. [CrossRef]
2. Faella, C.; Lima, C.; Martinelli, E.; Pepe, M.; Realfonzo, R. Mechanical and durability performance of sustainable structural concretes: An experimental study. *Cem. Concr. Compos.* **2016**, *71*, 85–96. [CrossRef]
3. Va'zquez, E. *Progress of Recycling in the Built Environment*; Springer: Berlin/Heidelberg, Germany, 2013. [CrossRef]
4. Hasanbeigi, A.; Price, L.; Lin, E. Emerging energy-efficiency and CO2emission-reduction technologies for cement and concrete production: A technical review. *Renew. Sustain. Energy Rev.* **2012**, *16*, 6220–6238. [CrossRef]
5. Behera, M.; Bhattacharyya, S.K.; Minocha, A.K.; Deoliya, R.; Maiti, S. Recycled aggregate from C&D waste & its use in concrete—A breakthrough towards sustainability in construction sector: A review. *Constr. Build. Mater.* **2014**, *68*, 501–516. [CrossRef]
6. Amario, M.; Rangel, C.S.; Pepe, M.; Toledo Filho, R.D. Optimization of normal and high strength recycled aggregate concrete mixtures by using packing model. *Cem. Concr. Compos.* **2017**, *84*, 83–92. [CrossRef]
7. Santana Rangel, C.; Amario, M.; Pepe, M.; Yao, Y.; Mobasher, B.; Toledo Filho, R.D. Tension stiffening approach for interface characterization in recycled aggregate concrete. *Cem. Concr. Compos.* **2017**, *82*, 176–189. [CrossRef]
8. Dong, W.; Wu, Z.; Zhou, X.; Dong, L.; Kastiukas, G. FPZ evolution of mixed mode fracture in concrete: Experimental and numerical. *Eng. Fail. Anal.* **2017**, *75*, 54–70. [CrossRef]
9. Bui, N.K.; Satomi, T.; Takahashi, H. Improvement of mechanical properties of recycled aggregate concrete basing on a new combination method between recycled aggregate and natural aggregate. *Constr. Build. Mater.* **2017**, *148*, 376–385. [CrossRef]
10. Bravo, M.; de Brito, J.; Evangelista, L.; Pacheco, J. Superplasticizer's efficiency on the mechanical properties of recycled aggregates concrete: Influence of recycled aggregates composition and incorporation ratio. *Constr. Build. Mater.* **2017**, *153*, 129–138. [CrossRef]

11. Pepe, M.; Toledo Filho, R.D.; Koenders, E.A.B.; Martinelli, E. A novel mix design methodology for Recycled Aggregate Concrete. *Constr. Build. Mater.* **2016**, *122*, 362–372. [CrossRef]
12. Dilbas, H.; Şimşek, M.; Çakir, Ö. An investigation on mechanical and physical properties of recycled aggregate concrete (RAC) with and without silica fume. *Constr. Build. Mater.* **2014**, *61*, 50–59. [CrossRef]
13. Mehta, P.K.; Monteiro, P.J.M. *Concrete: Microstructure, Properties and Materials*; McGraw Hill: New York, NY, USA, 2006.
14. Li, W.; Pour-Ghaz, M.; Castro, J.; Weiss, J. Water Absorption and Critical Degree of Saturation Relating to Freeze-Thaw Damage in Concrete Pavement Joints. *J. Mater. Civ. Eng.* **2012**, *24*, 299–307. [CrossRef]
15. Kou, S.C.; Poon, C.S. Effect of the quality of parent concrete on the properties of high performance recycled aggregate concrete. *Constr. Build. Mater.* **2015**, *77*, 501–508. [CrossRef]
16. Bulatović, V.; Melešev, M.; Radeka, M.; Radonjanin, V.; Lukić, I. Evaluation of sulfate resistance of concrete with recycled and natural aggregates. *Constr. Build. Mater.* **2017**, *152*, 614–631. [CrossRef]
17. Kwan, W.H.; Ramli, M.; Kam, K.J.; Sulieman, M.Z. Influence of the amount of recycled coarse aggregate in concrete design and durability properties. *Constr. Build. Mater.* **2012**, *26*, 565–573. [CrossRef]
18. Gomes, M.; De Brito, J. Structural concrete with incorporation of coarse recycled concrete and ceramic aggregates: Durability performance. *Mater. Struct.* **2009**, *42*, 663–6675. [CrossRef]
19. Levy, S.M.; Helene, P. Durability of recycled aggregates concrete: A safe way to sustainable development. *Cem. Concr. Res.* **2004**, *34*, 1975–1980. [CrossRef]
20. Bassuoni, M.T.; Nehdi, M.L. Durability of self-consolidating concrete to sulfate attack under combined cyclic environments and flexural loading. *Cem. Concr. Res.* **2009**, *39*, 206–226. [CrossRef]
21. Zeng, Q.; Fen-Chong, T.; Li, K. Freezing behavior of cement pastes saturated with NaCl solution. *Constr. Build. Mater.* **2014**, *59*, 99–110. [CrossRef]
22. Liu, Z.; Hansen, W. Freeze–thaw durability of high strength concrete under deicer salt exposure. *Constr. Build. Mater.* **2016**, *102*, 478–485. [CrossRef]
23. Sun, Z.; Scherer, G.W. Effect of air voids on salt scaling and internal freezing. *Cem. Concr. Res.* **2010**, *40*, 260–270. [CrossRef]
24. Farnam, Y.; Wiese, A.; Bentz, D.; Davis, J.; Weiss, J. Damage development in cementitious materials exposed to magnesium chloride deicing salt. *Constr. Build. Mater.* **2015**, *93*, 384–392. [CrossRef]
25. Wan, X.S.; Lai, Y.M. Experimental study on freezing temperature and salt crystal precipitation of sodium sulphate soulotion and sodium sulphate saline soil. *Chin. J. Geotech. Eng.* **2013**, *35*, 7. (In Chinese)
26. Ghorbel, E.; Wardeh, G. Influence of recycled coarse aggregates incorporation on the fracture properties of concrete. *Constr. Build. Mater.* **2017**, *154*, 51–60. [CrossRef]
27. Chen, G.M.; Yang, H.; Lin, C.J.; Chen, J.F.; He, Y.H.; Zhang, H.Z. Fracture behaviour of steel fibre reinforced recycled aggregate concrete after exposure to elevated temperatures. *Constr. Build. Mater.* **2016**, *128*, 272–286. [CrossRef]
28. Gesoglu, M.; Güneyisi, E.; Öz, H.Ö.; Taha, I.; Yasemin, M.T. Failure characteristics of self-compacting concretes made with recycled aggregates. *Constr. Build. Mater.* **2015**, *98*, 334–344. [CrossRef]
29. Guo, Y.C.; Zhang, J.H.; Chen, G.; Chen, G.M.; Xie, Z.H. Fracture behaviors of a new steel fiber reinforced recycled aggregate concrete with crumb rubber. *Constr. Build. Mater.* **2014**, *53*, 32–39. [CrossRef]
30. *GB/T 50082-2009*; Standard for Test Methods of Long-Term Performance and Durability of Ordinary Concrete. Ministry of Housing and Urban-Rural Development: Beijing, China, 2009. (In Chinese)
31. Abbaszadeh, R.; Modarres, A. Freeze-thaw durability of non-air-entrained roller compacted concrete designed for pavement containing cement kiln dust. *Cold Reg. Sci. Technol.* **2017**, *141*, 16–27. [CrossRef]
32. Liu, Z.; Hansen, W. Pore damage in cementitious binders caused by deicer salt frost exposure. *Constr. Build. Mater.* **2015**, *98*, 204–216. [CrossRef]
33. Jin, S.; Zheng, G.; Yu, J. A micro freeze-thaw damage model of concrete with fractal dimension. *Constr. Build. Mater.* **2020**, *257*, 119434. [CrossRef]
34. Eriksson, D.; Wahlbom, D.; Malm, R.; Fridh, K. Hygro-thermo-mechanical modeling of partially saturated air-entrained concrete containing dissolved salt and exposed to freeze-thaw cycles. *Cem. Concr. Res.* **2021**, *141*, 106314. [CrossRef]
35. RILEM Draft Recommendation (TC50-FMC). Determination of fracture energy of mortar and concrete by means of three-point bend test on notched beams. *Mater. Struct.* **1985**, *18*, 285–290.
36. *GB/T 50081-2002*; Standard for Test Method of Mechanical Properties on Ordinary Concrete. Ministry of Housing and Urban-Rural Development: Beijing, China, 2002. (In Chinese)
37. Kequan, Y.; Jiangtao, Y.; Zhoudao, L.; Qingyang, C. Determination of the softening curve and fracture toughness of high-strength concrete exposed to high temperature. *Eng. Fract. Mech.* **2015**, *149*, 156–169. [CrossRef]
38. Neville, A. The confused world of sulfate attack on concrete. *Cem. Concr. Res.* **2004**, *34*, 1275–1296. [CrossRef]
39. Whittaker, M.; Black, L. Current knowledge of external sulfate attack. *Adv. Cem. Res.* **2015**, *27*, 532–545. [CrossRef]
40. Lothenbach, B.; Bary, B.; Le Bescop, P.; Schmidt, T.; Leterrier, N. Sulfate ingress in Portland cement. *Cem. Concr. Res.* **2010**, *40*, 1211–1225. [CrossRef]
41. Jiang, L.; Niu, D.; Yuan, L.; Fei, Q. Durability of concrete under sulfate attack exposed to freeze–thaw cycles. *Cold Reg. Sci. Technol.* **2015**, *112*, 112–117. [CrossRef]

42. Kosior-Kazberuk, M. Variations in fracture energy of concrete subjected to cyclic freezing and thawing. *Arch. Civ. Mech. Eng.* **2013**, *13*, 254–259. [CrossRef]
43. Ferreira, M.; Kuosa, H.; Leivo, M.; Holt, E. Concrete performance subject to coupled deterioration in cold environments. *Nucl. Eng. Des.* **2017**, *323*, 228–234. [CrossRef]